J. Biochem. 2009;145(2)199–206
doi:10.1093/jb/mvn157

Structural Insights of the Nucleotide-Dependent Conformational Changes of *Thermotoga maritima* MutL Using Small-Angle X-ray Scattering Analysis

Tae Gyun Kim[1], Hyung Jin Cha[2], Hyung Ju Lee[1], Seong-Dal Heo[1], Kwan Yong Choi[2], Ja Kang Ku[1] and Changill Ban[1,*]

[1]Department of Chemistry; and [2]Department of Life Science, Pohang University of Science and Technology, Pohang, Gyungbuk 790-784, Korea

Received October 20, 2008; accepted November 14, 2008; published online November 23, 2008

MutL is required to assist the mismatch repair protein MutS during initiation of the methyl-directed mismatch repair (MMR) response in various organisms ranging from prokaryotes to eukaryotes. Despite this necessity, the inherent propensity of MutL to aggregate has led to significant difficulties in determining its biological relationship with other MMR-related proteins. Here, we perform analysis on the thermostable MutL protein found in *Thermotoga maritima* MSB8 (TmL). Size exclusion chromatographic analysis indicates the lack of aggregated forms with the exception of a dimeric TmL. Small-angle X-ray scattering (SAXS) analysis reveals that the solution structures of the full-length TmL and its corresponding complexes with nucleotides and ssDNA undergo conformational changes. The elucidated TmL SAXS model is superimposed to the crystal structure of the C-terminal domain of *Escherichia coli* MutL. In addition, the N-terminal SAXS model of TmL exists as monomeric form, indicating that TmL has a structurally flexible N-terminal domain. TmL SAXS analysis can suggest a considerable possibility on a new 3D view of the previously unresolved full-length MutL molecule.

Key words: conformational change, *Escherichia coli* MutL, Methyl-directed mismatch repair, Small-angle X-ray scattering, *Thermotoga maritima* MSB8 MutL.

Abbreviations: MMR, Methyl-directed mismatch repair; TmL, *Thermotoga maritima* MSB8 MutL; SAXS, Small-angle X-ray scattering; DLS, Dynamic light scattering.

The methyl-directed mismatch repair (MMR) system is an essential process for correcting errors generated during DNA replication in living organisms from prokaryotes to eukaryotes (*1–2*). Three essential proteins from the prokaryotic MMR system, MutS, MutL and MutH, perform crucial roles in detecting mismatched DNA, initiating the repair pathway, and activating other MMR related proteins (*3–5*). The inactivation of the human MMR system affects the genetic integrity of the chromosomes, the genomic stability and the intracellular mutation rate, resulting in increased susceptibility of humans to the development of various cancers, such as hereditary nonpolyposis colorectal cancer (*6*).

With respect to MMR-related proteins, MutL physically interacts with MutS to form the MutL–MutS complex, which can then recognize a mispaired or unpaired region in a DNA duplex and subsequently stimulate MutH, an enzyme that cleaves DNA at a hemi-methylated GATC site (*4*, *7*). MutL also stimulates the loading of DNA helicase II at nicks in genomic DNA, thereby increasing the efficiency of DNA unwinding (*8*, *9*), in addition to binding to the β subunit and the clamp loader (δ,δ′ and γ subunits) of DNA polymerase III (*10*). Modrich *et al*. (*11*) described the functions of the eukaryotic MutL homologues in the human MMR system, such as the hetero-dimeric MutLα. Unlike *Escherichia coli* MutL, MutLα has an intrinsic endonuclease activity that is dependent upon its interaction with ATP, mispaired DNA, replication factor C, proliferating cell nuclear antigen, the replication clamp loader and MutS homologues (*11*, *12*). Despite many previous functional studies on MutL proteins that have revealed their essential role in the MMR system, the biological functions of MutL and its homologues still remain enigmatic.

One of the difficulties in performing detailed functional studies of these MMR-related proteins is derived from the tendency of MutL to self-aggregate in solution. Structurally corroborated data for MutL may contribute to the understanding of the correlation between its structure and function. In this study, we present the solution structure of the thermostable MutL protein from the fully sequenced hyper-thermophilic bacterium *T. maritima* MSB8 using small-angle X-ray scattering (SAXS) analysis. The superimposition of the SAXS-based TmL model on the crystal structure of *E. coli* MutL elucidated a 3D view of the previously unresolved full-length MutL homologue.

MATERIALS AND METHODS

Protein Preparations—The *T. maritima* MSB8 (*13*) genomic DNA (GenBank accession No. AE000512) was

*To whom correspondence should be addressed: Tel: +82-54-279-2127, Fax: +82-54-279-3399, E-mail: ciban@postech.ac.kr

kindly provided by Professor Yu-Ryang Pyun (Yonsei University, Korea). The open reading frames of the *mut*L (1551 bp) gene were amplified from the *T. maritima* MSB8 genomic DNA by PCR with i-pfu polymerase (iNtRON Biotechnology Inc.) using gene specific primers (F: 5′-CGCGGATCCGTGGAGAGGTGTTCTGTTTT-3′ and R: 5′-CCCAAGCTTTTAACGCTCGAAAAATCGG TC-3′). The PCR-amplified genes were cloned into the bacterial expression vector pET-28aTEV [modified pET-28a (Novagen, Germany) with an inserted TEV (Tabacco Etch Virus) protease recognition site] at the appropriate restriction enzyme sites. The clone was confirmed by DNA sequencing. TmL was over-expressed using pET-28aTEV in the BL21 Star™ (DE3) (Invitrogen, USA) strain at 37°C. Four liters of TmL were grown at 37°C in Luria-Bertani medium containing 50 μg/ml kanamycin. Supernatant from the lysed cell mixture was applied to a nickel-nitrilotriacetic acid (Ni-NTA, GE Healthcare, Denmark) affinity column, which had been pre-equilibrated with nickel ions and lysis buffer (20 mM Tris–HCl, pH 8.0, 500 mM NaCl, 0.5 mM β-mercaptoethanol, 5% glycerol and 5 mM imidazole). His-tagged fragments of TmL and its mutants were cleaved by incubation of TEV protease with the corresponding protein fractions at room temperature for 10 h. Solutions of the cleaved TmL and its mutants were then re-loaded onto the Ni-NTA column, and the flow through was then further purified using a Hitrap Heparin column (GE Healthcare, Denmark) equilibrated with buffer I [50 mM Hepes–KOH, pH 7.0, 100 mM KCl, 1 mM dithiothreitol (DTT), 1 mM ethylenediaminetetraacetic acid (EDTA)] and eluted with buffer I using a linear gradient of 0.5 M KCl. TmL was finally applied to a Superdex 200 HR gel filtration column (GE Healthcare, Denmark) equilibrated with buffer II (20 mM Tris–HCl, pH 8.0, 200 mM NaCl, 1 mM DTT, 1 mM EDTA, 5% glycerol). Purified TmL was concentrated using an Ultracel Amicon YM-10 (Millipore, USA) and was shown to be 99% pure using sodium dodecylsulfate polyacrylamide gel electrophoresis (SDS–PAGE). The concentration of TmL was determined using the theoretical extinction coefficient of TmL (36 995 $M^{-1}cm^{-1}$). To determine the molecular size of the native protein, standard proteins, including apo ferritin (440 kDa), catalase (232 kDa) and bovine serum albumin (BSA, 66 kDa in its monomeric form), were loaded onto the Superdex 200 HR column equilibrated with buffer II. The N-terminal portion of *E. coli* MutL (residues 1–331) was purified according to previously reported procedures (*14*, *15*). The N-terminal domains of TmL (1–344) were expressed and purified using the same methods as those described for the apo-TmL.

Determination of the Molecular Morphologies Using Dynamic Light Scattering (DLS)—To measure the thermo-stability of the apo-TmL, the Zetasizer Nano system was used. Sample detections were performed in low volume glass cuvettes. A latex standard with a uniform particle size of 20 nm was applied to evaluate the accuracy of the measurement. The mean hydrodynamic diameter (d) was estimated using the Debye–Einstein–Stokes equation, $D = k_B T/6\pi\eta r$ (k_B is the Boltzman constant, T is the absolute temperature, η is the viscosity of the dispersing medium and D is the apparent diffusion coefficient). The conditions used to determine the size of TmL were as follows: temperatures of 25, 35, 45 and 55°C; a count rate of 285.8 kcps; a 60 s time duration; a 90° detection angle and a viscosity value of 0.891 cP (dilute water solution).

SAXS Data Acquisition—SAXS data were collected at the BL45XU beamline at the RIKEN Institute, SPring-8 (Japan). The incident wavelength was 1.0 Å, and the incident flux at the sample position was 10^{12} photons/second with dimensions of 0.5 mm × 0.2 mm. The distance between the samples and the XR-II + CCD (X-ray image intensifier with CCD) detector system was 2160.186 mm. A chamber and a pixel size of 0.1 mm × 0.1 mm were used. The data acquisition was done within an S-range of 0.006 to 0.23 $Å^{-1}$ (S is the scattering vector: $S = 4\pi\sin\theta/\lambda$, where 2θ is the scattering angle and λ is the wavelength), with a sample exposure time of 100 s. To determine the length of time required for data collection, scattering from the buffer alone was collected both before and after adding the protein sample. Both the pre- and post-sample buffer data were subtracted from the protein sample scattering data. The sample buffer was composed of 20 mM Tris–HCl (pH 7.6), 200 mM KCl, 10 mM DTT, 1 mM EDTA, 5 mM $MgCl_2$ and 5% glycerol. Here, 5% glycerol was added in order to serve as a radiation scavenger. The SAXS data for the thermostable TmL were collected at concentrations of 5 mg/ml at 45°C. Buffer and sample volumes of 30 μl were used. To further evaluate the conformational changes, TmL (5 mg/ml, 41 μM per dimer) was reacted with nucleotides (ATP, ADP and ADPnP; 1 mM each) and a 30-mer ssDNA substrate (100 μM, 2.5-fold of TmL molar ratio) before SAXS data were collected at 45°C. In order to assume uniform density distributions for the TmL–nucleotide and the TmL–ssDNA reactants, the same concentrations of nucleotides and ssDNA were added to the sample buffer, indicating that nucleotides are added to remove the error value on scattering data of free nucleotides. An assessment of the initial scattering profile was performed using the program PRIMUS (*16*, *17*). The radii of gyration (R_g) were determined by fitting the intensity profiles under the Guinier approximation as implemented by PRIMUS. The Guinier approximation assumes that, at a very small angle, the intensity is represented by the expression $I(S) = I(0)\exp(-4\pi^2 R_g^2 S^2/3)$, where $I(0)$ is the forward-scattering intensity at a zero angle. These parameters were also computed from the entire scattering pattern using the indirect transform program GNOM (*18*), which also provides a pair-wise distribution function for the interatomic vector, $P(r) = (1/2\pi^2)I(q)q{\cdot}r\ \sin(q{\cdot}r)\mathrm{d}q$. The inverse Fourier transform of $I(q)$ yields $P(r)$, the frequency of vector lengths connecting small-volume elements within the entire volume of the scattering particle. $P(r)$ approaches zero at the momentum linear dimension of the particle, $D_{max}{\cdot}R_g$ and the forward scatter, $I(0)$, were calculated from the second and zeroth moments of $P(r)$, respectively.

Scattering Data Analysis and Modelling—A 3D scattering shape for the apo-TmL and its complexes with nucleotides and ssDNA, which best fit the corresponding SAXS intensity data, was generated using the

DAMMIN program (*19*). Structure regenerations using no shape or 2-fold symmetry bias were used to model all data sets. DAMMIN represents the particle as a collection of densely packed beads inside a sphere with the diameter D_{max}. The readout low-resolution shapes for the TmL models were aligned with the known crystal structures of the N- and C-terminal domains of *E. coli* MutL (pdb no 1BKN and 1X9Z, respectively) using SUPREF program (*20*). The refined rigid body models obtained from the SAXS data for apo-TmL and its complexes with nucleotides and ssDNA were generated using the program PyMOL.

RESULTS AND DISCUSSION

Sequence Comparison Between TmL and E. coli MutL—TmL is composed of 516 residues, whereas the known *E. coli* MutL protein has 615 residues. Sequence alignment between TmL and *E. coli* MutL indicates 27.2% sequence identity and 41% sequence homology (Fig. 1). Although the two proteins share highly homologous N-terminal ATPase and C-terminal dimerization domains, the linking region between these two domains in sequence alignment of TmL and *E. coli* MutL is different with size. Yang *et al*. (*21*) suggested that residues 432–615 of *E. coli* MutL comprise the minimal folded region that is essential for dimerization and that the 100 amino acids encompassing residues 332–431 form an extended linker, as suggested by secondary structure predictions. The N-terminal Walker's A-type ATPase domain of *E. coli* MutL binds directly to ADPnP and interacts with several amino acid residues, such as Asp58, Ser78, Lys79, Phe94, Ala100 and Thr143, and with Mg^{2+} ions and water molecules (*14*,*15*) (Fig. 1). These nucleotide-interacting residues of *E. coli* MutL are well conserved with those residues of TmL, based on

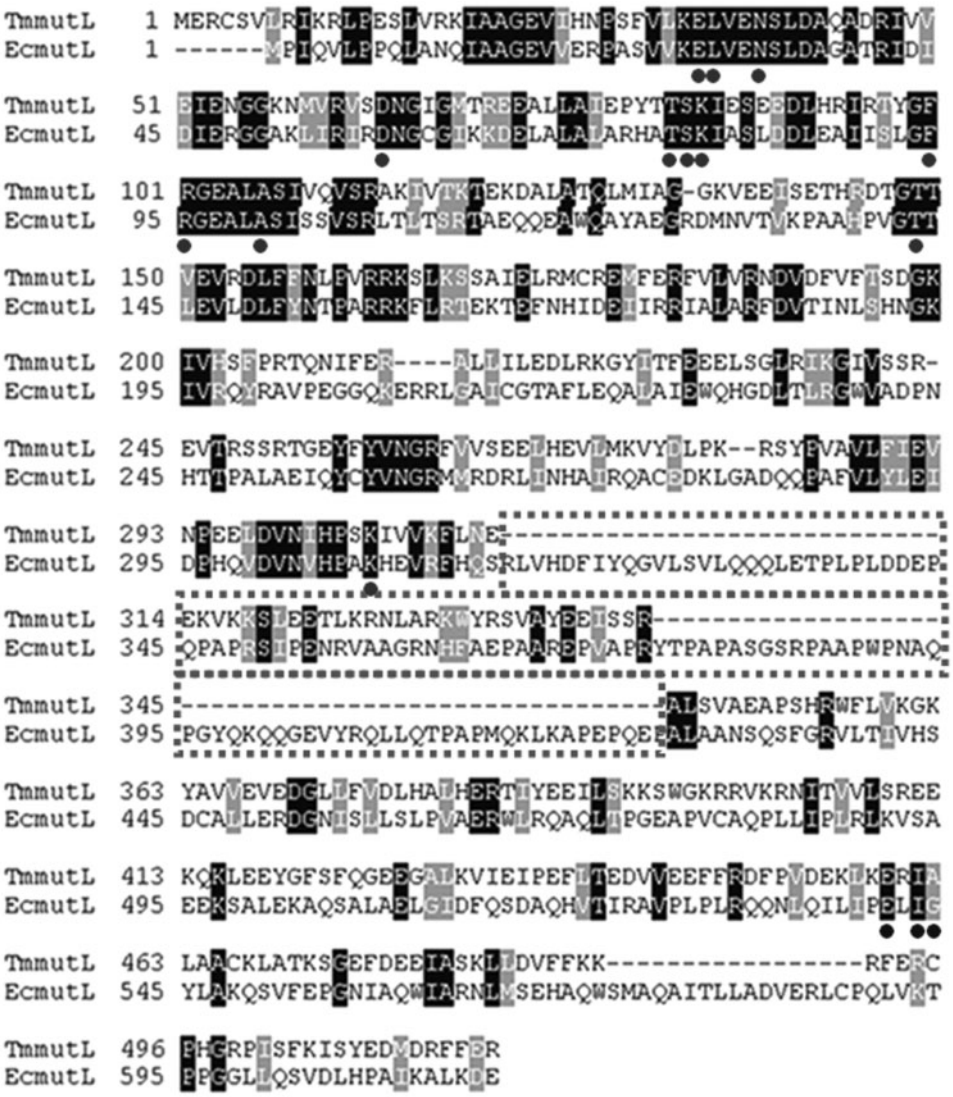

Fig. 1. **The amino acid sequence alignment of TmL and *E. coli* MutL.** The amino acid sequence alignment between TmL and *E. coli* MutL was generated using the multiple alignment programs GOR and CLASTALW (http://www.ebi.ac.uk/Tools/clustalw2/index.html). Black circles indicate the ATP-binding-related residues and the dimeric-interface-related residues (residues 459, 461 and 462), respectively. The dash-line box indicates the nonstructural domain.

alignment analysis. Also, it is known that two pairs of α-helices at the dimer interface of the C-terminal dimerization domain of *E. coli* MutL play an important role in the formation of the nucleotide binding site (*21*). The secondary structure prediction program GOR (*22*) provides the corresponding α-helices of TmL. This finding shows that the matched regions in both proteins may account for some of the functional similarity between *E. coli* MutL and TmL. Based on the sequence alignment, it can be readily assumed that the shorter non-structural domain (NSD) found in TmL, in comparison to the corresponding domain in *E. coli* MutL, may account for its more stable secondary structure.

Thermostable Dimeric TmL Protein—We used TmL that was expressed as an *E. coli* recombinant protein under an isopropyl β-D-thiogalactopyranoside-induced T7 promoter system. The purified TmL was about 99% pure based on SDS–PAGE analysis (Fig. 2A). The apparent molecular weight of TmL was estimated by SDS–PAGE to be approximately 60.5 kDa, consistent with the molecular weight of 59.7 kDa that has been theoretically calculated from the amino acid sequence of TmL. To determine the oligomeric state of the native protein, purified TmL was loaded onto a Superdex 200 HR chromatography column that was calibrated with standard proteins such as apo-ferritin (440 kDa), catalase (232 kDa) and bovine serum albumin (BSA, 66 kDa in its monomeric form). A previous report indicated an anomaly regarding the oligomeric state of the *E. coli* MutL in solution (*14*). In this previous report, elution of *E. coli* MutL from the Superdex 200 HR gel filtration column displayed two peaks, a major peak corresponding to a complex greater than 200 kDa and a minor peak corresponding to a complex of less than 200 kDa (*14*), indicating the aggregated formation of *E. coli* MutL. However, unlike *E. coli* MutL, the elution of TmL reported herein showed only one peak, in the range of 120 and 150 kDa, indicating that dimeric TmL does not form a similar aggregated complex as observed with *E. coli* MutL (Fig. 2B). The TmL used in our experiments was re-heated at 55°C for an hour and then applied in Superdex 200 HR gel filtration chromatography (data not shown). The re-heated TmL also retained a thermostable dimeric form that resembled the freshly prepared TmL. To further assess the thermostability of TmL, dynamic light scattering (DLS) measurements employed a Zetasizer Nano ZS system (Malvern Ins.). DLS results indicated that the hydrodynamic diameter and percent scattering intensity retained their reproducibility over a range of temperatures from 25°C to 55°C (Fig. 3). Therefore, the dimeric TmL possessed the thermostable characteristics.

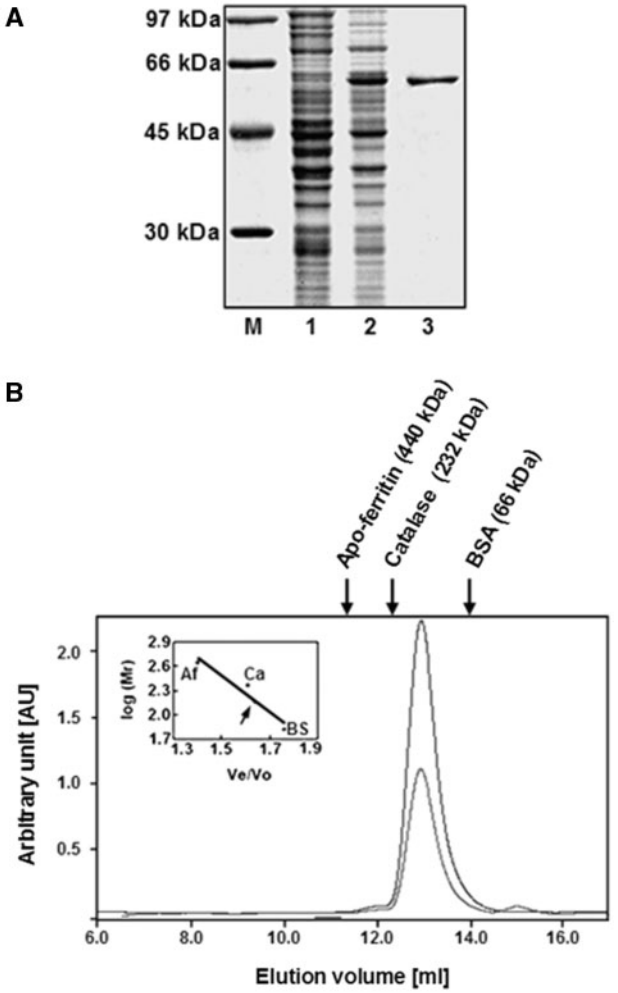

Fig. 2. **SDS–PAGE and size exclusion analyses of TmL.** (A) SDS–PAGE analysis for TmL. Lane 1 is the low molecular weight marker. Lanes 2 and 3 are the crude extract before and after IPTG induction, respectively. Lane 4 is the final purified TmL. (B) Size exclusion chromatographic analysis of the dimeric TmL using Superdex 200 HR gel filtration column. In order to calculate the molecular weight of TmL, several calibrated standard proteins [apo ferritin (440 kDa), catalase (232 kDa) and bovine serum albumin (BSA, 66 kDa in monomer)] were loaded onto the Superdex 200 HR gel filtration column. The inset shows that the molecular weight for TmL was calculated from a plot of log values of molecular weight against V_e/V_o, where V_e is the protein-eluted volume and V_o is the column-void volume (volume fitted by Blue-dextran). Af, Ca and BS indicate apo-ferritin, catalase, and BSA, respectively. The arrow represents the calculated log value for the TmL molecular weight.

Various Conformational Changes Observed for the TmL SAXS Structures in the Presence and Absence of Nucleotides and ssDNA—In order to elucidate the solution structure of the thermostable TmL, SAXS analysis was performed at 45°C using 5 mg/ml of TmL. As shown in Fig. 4A, the overlay of the scattering curves for TmL and its complexes with nucleotides and ssDNA were also collected at 45°C. The shape of the molecule can be reconstructed from the analytical SAXS curve (*23–25*). The scattering results were analysed by the low angle region in the first and last frames of the SAXS data, and they did not show an increase in the radius of gyration (R_g), indicating that aggregation did not occur during the SAXS analysis. In order to represent the lowest S range, we showed the Guinier approximations of the apo-TmL protein and its complexes with nucleotides and ssDNA, supporting the initial scattering data in the S range from 0.006 to 0.23 $Å^{-1}$ (Supplementary Fig. S1). The scattering data were then transformed to generate a pair-wise distribution function $P(r)$ for predicting the TmL SAXS

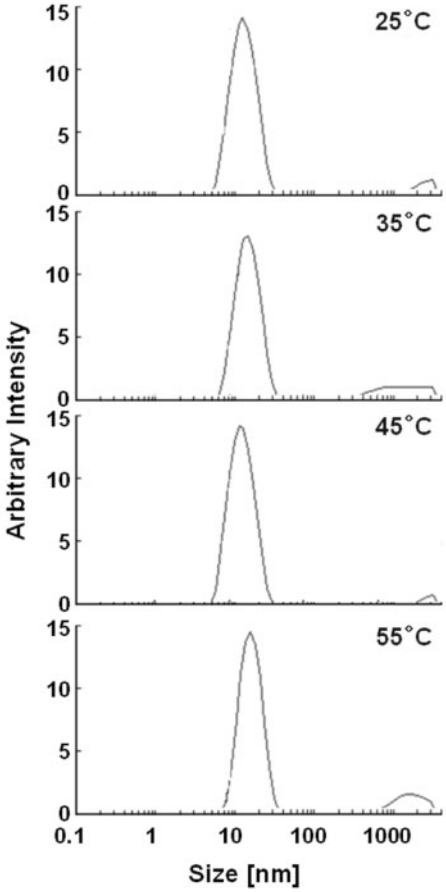

Fig. 3. **DLS results for TmL at various temperatures (25, 35, 45 and 55°C).** The percent intensity (*y*-axis) is the percentage of the majority of peaks. For each sample, three runs of 20 individual measurements were performed.

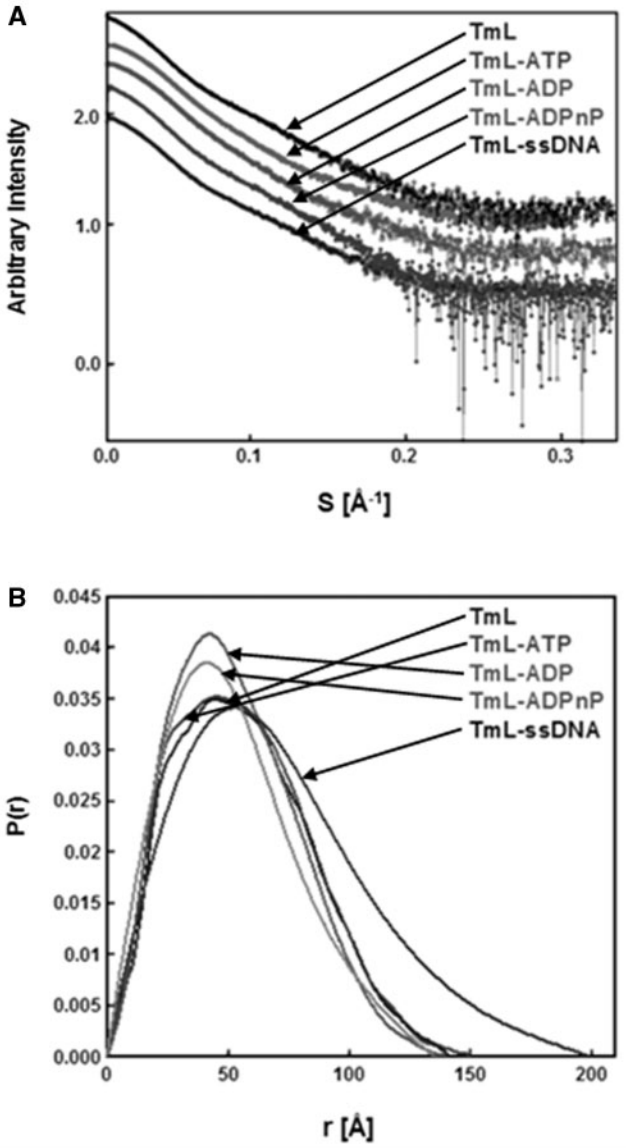

Fig. 4. **Initial SAXS scattering curve and *P*(*r*) function of TmL and its complexes with nucleotides and ssDNA.** (A) SAXS scattering curves for the apo-TmL, the TmL–ATP complex, the TmL–ADP complex, the TmL–ADPnP complex and the TmL–ssDNA complex. The **S** (*x*-axis) value is the scattering vector. (B) The comparative pair-wise vector length distribution curves [*P*(*r*)] of the apo-TmL and its complexes with nucleotides and ssDNA.

models (Fig. 4B). Based on the Guinier approximations and GNOM analysis, the R_g and D_{max} values were determined and are summarized in Table 1. The $P(r)$ curve of the apo-TmL indicated that the D_{max} was 142 Å and the R_g was calculated to be 44.7 ± 0.7 Å. According to a comparison of the R_g and D_{max} values, while TmL–nucleotide complexes had similar R_g values to the apo-TmL, the TmL–ssDNA complex had larger R_g values (53.0 ± 1.0 Å) than that of apo-TmL. These findings suggest that TmL complexed with nucleotides or ssDNA had different conformations when compared to the apo-TmL protein.

The low resolution structures of the TmL protein and its protein complexes with nucleotides and ssDNA were constructed from the $P(r)$ curve using the DAMMIN program. In the initial modelling studies, implemented with no shape bias, TmL was predicted to have a 2-fold symmetry due to the dimeric form that was indicated from the size exclusion chromatographic analysis. Final structural modelling using DAMMIN was performed using 2-fold symmetry. In Fig. 5A, the SAXS results showed the full-length MutL structure, which possesses a 2-fold symmetry with an extended and reversed W-shaped conformation, similar to that of a flying bird. The results from the scattering profile appear to be reliable since we do not observe the existence of the insoluble form of TmL that was shown in the DLS analyses. One possible reason for the extended conformation of the TmL SAXS model was the large ratio of the D_{max} value to the R_g value ($D_{max} \approx 3.2 R_g$). This result resembled the aggregation observed during the SAXS measurement, but comparison of the low angle region of the first and last frames of the SAXS data does not show a corresponding increase in the R_g value. Therefore, no aggregation occurred during the SAXS experiments.

Table 1. **SAXS data parameters from the Guinier approximation and GNOM analysis.**

Samples	R_{pre}	R_{cal}	D_{max}
TmL	46.5 ± 0.2	44.7 ± 0.7	142
TmL–ATP	46.3 ± 0.1	45.0 ± 0.9	150
TmL–ADP	41.9 ± 0.2	42.7 ± 0.2	140
TmL–ADPnP	40.9 ± 0.1	41.5 ± 0.4	136
TmL–ssDNA	49.3 ± 0.4	48.1 ± 0.5	192

R_{pre} was calculated using the Guinier approximation. R_{cal} and D_{max} values were calculated from the $P(r)$ function by GNOM. D_{max} is the longest distance of SAXS models resulting from DAMMIN.

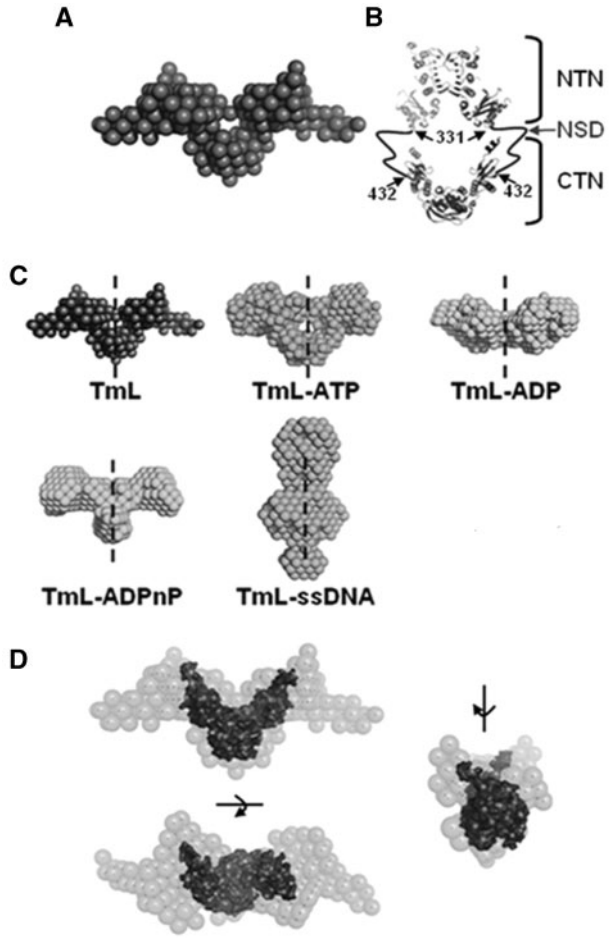

Fig. 5. **The SAXS models for TmL and its complexes with nucleotides and ssDNA.** (A) The best-fit ab initio model for the apo-TmL. (B) The connecting model between crystal structures of the N- (NTN) and the C-terminal (CTN) domains of *E. coli* MutL. The dashed line is the NSD (non-structural domain, residues 332–431). (C) The SAXS models for the apo-TmL and its complexes with nucleotides (ATP, ADP and ADPnP) and ssDNA shown using a spaced-filled dummy atom model (DAM). The vertical dashed lines represent the 2-fold symmetry of the SAXS models. (D) Automated fits of the high resolution crystal structure (pdb No. 1X9Z) of the C-terminal domain (deep grey) of E. coli MutL within the low resolution apo-TmL SAXS model (grey).

While Fig. 5B represents the presumed model for the overall structure of the *E. coli* MutL protein (*21*), the apo-TmL SAXS model indicated a different structure than that proposed by the *E. coli* MutL model. For *E. coli* MutL, previous data have demonstrated that the presence of nucleotides induces conformational changes in the full-length *E. coli* MutL and its mutant forms by using both cross-linking and size exclusion chromatographic analyses (*14*, *21*). We showed here that the TmL–ssDNA complex had a close-elongated conformation, while other TmL–nucleotides complexes had relatively open formations (Fig. 5C), indicating that the TmL protein undergoes significant conformational changes in the presence of nucleotides and ssDNA. Interestingly, the TmL–DNA model resembled the fully dimeric form, indicating that the ssDNA-bound TmL may have a similar globular conformation to that of the presumed model for *E. coli* MutL. It is known that proteins containing ATP hydrolytic and DNA binding activities have a large conformational transition in the presence of nucleotide and DNA. This means that both the nucleotide- and DNA-induced conformational changes of TmL can be generated to investigate the high-resolution structure of the full-length MutL and potentially other intermediate conformations in the MMR system.

Superposition of the TmL SAXS Structure and the Crystal Structure of E. coli MutL—In order to compare the structure of TmL with that of *E. coli* MutL, superimposition analysis using the program SUPREF was performed between the dummy atom model (DAM) for TmL and each N-/C-terminal representation of the structure of *E. coli* MutL. However, the monomeric *E. coli* N-terminal MutL structure (pdb no 1B62) did not superimpose well with the TmL SAXS model. The final overlay demonstrated that the *E. coli* C-terminal MutL structure (pdb no 1X9Z) fits well with the SAXS-based TmL model, but the N-terminal region of TmL became disjoined (Fig. 5D). This superimposed model indicated a different structural morphology than that model predicted for the entire structure of *E. coli* MutL.

To elucidate the structure of the N-terminal domain (1–344) of TmL, SAXS experiments were performed. As shown in Fig. 6, the N-terminal domain of TmL did not form a dimer, unlike the homo-dimer interaction observed for the N-terminal domain of *E. coli* MutL (*14*, *21*). The TmL SAXS model seemed to be observed in disjoined N-terminal domains, indicating that individual N-termini of the apo-TmL do not form dimers in solution. However, based on the SAXS models of the TmL and the nucleotide- and ssDNA–TmL complexes, we confirmed conformational changes in the TmL protein, such as dimerization of the N-terminal region. Therefore, these observations indicated that TmL has structurally flexible regions, especially in the N-terminal domain, allowing a certain amount of conformational flexibility in the presence of nucleotides or DNA. Thus, the TmL SAXS models presented here are the first to show the significant differences in structural conformation that was not observed in the *E. coli* MutL.

In conclusion, we have presented conformational transition models for MutL based on the solution structure of the full-length MutL homologue induced by both nucleotides and ssDNA. Analysis of these superimposed structures of the SAXS-based TmL model and the crystal structure of *E. coli* MutL has revealed a novel 3D view of the previously unknown full-length MutL molecule.

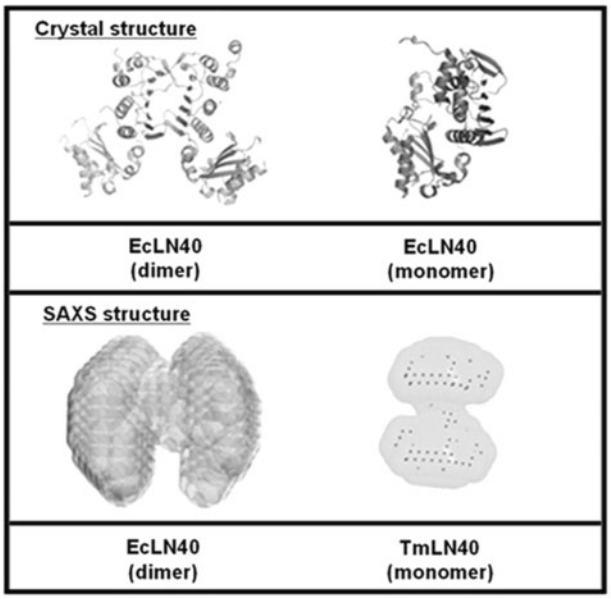

Fig. 6. **Structural comparison between TmLN40 and EcLN40.** The SAXS models for the N-terminal domains of *E. coli* MutL (residues 1–331) and TmL (residues 1–344) indicated as EcLN40 and TmLN40, respectively. The crystal structure of EcLN40 (pdb no 1BKN) is a dimer. The monomeric form of EcLN40 is indicated as pdb no 1B62.

Moreover, in order to completely understand the MutL structure, it is necessary to define the high-resolution structure of MutL. From this perspective, the TmL SAXS solution structures will provide important clues not only to understand the atomic resolution structure of the MutL protein but also to elucidate the functional correlations among the prokaryotic and eukaryotic MutL homologues and the MMR-related proteins.

SUPPLEMENTARY DATA

Supplementary data are available at *JB* online.

ACKNOWLEDGEMENTS

The authors wish to thank Professor Sam-Yong Park and Satoru Unzai for their greatly appreciated comments, Young-Ho Yoon for helping with the Zetasizer Nano system at Yokohama City University in Japan and Dr Kazuki Ito for technical assistance and helpful discussions at BL45XU beamline with approval of RIKEN Spring-8 Center (Proposal No. 20070154).

FUNDING

This work was supported by grants from the KOSEF through the Center for Integrated Molecular System at POSTECH (grant number: R11-2000-070-070010), the Korea Health Industry Development Institute (grant number: A020605), the Korea Health Industry Development Institute through Healthcare and Biotechnology Development Program (grant number: A050426) and the Korea Research Foundation Grant (KRF-2008-314-C00218).

CONFLICT OF INTEREST

None declared.

REFERENCES

1. Lyer, R.R., Plucinnik, A., Burdett, V., and Modrich, P.L. (2006) DNA Mismatch Repair: Functions and Mechanisms. *Chem. Rev.* **106**, 5–8
2. Yang, W., Junop, M., Ban, C., Obmolova, G., and Hsieh, P. (2001) DNA Mismatch Repair: From Structure to Mechanism. *Cold Spring Harbor Symp. Quant. Biol.* **65**, 225–232
3. Yang, W. (2000) Structure and functions of mismatch repair proteins. *Mutat. Res.* **460**, 245–256
4. Junop, M., Yang, W., Funchain, P., Clendenin, W., and Miller, J. (2003) *In vitro* and *in vivo* studies of MutS, MutL and MutH mutants: correlation of mismatch repair and DNA recombination. *DNA Repair* **2**, 387–405
5. Jun, S., Kim, T.G., and Ban, C. (2006) DNA mismatch repair system. Classical and fresh roles. *FEBS J.* **273**, 1609–1619
6. Jascur, T. and Boland, R. (2006) Structure and function of the components of the human DNA mismatch repair system. *Int. J. Cancer* **119**, 2030–2035
7. Heo, S.-D., Cho, M., Ku, J.K., and Ban, C. (2007) Steady-state ATPase activity of *E. coli* MutS modulated by its dissociation from heteroduplex DNA. *Biochem. Biophys. Res. Comm.* **364**, 264–269
8. Mechanic, L.E., Frankel, B.A., and Matson, S.W. (2000) *Escherichia coli* MutL loads DNA helicase II onto DNA. *J. Biol. Chem.* **275**, 38337–38346
9. Maston, S.W. and Robertson, A.B. (2006) The UvrD helicase and its modulation by the mismatch repair protein MutL. *Nucleic Acids Res.* **34**, 4089–4097
10. Li, F., Liu, Q., Chen, Y.-Y., Yu, Z.-N., Zhang, Z.-P., Zhou, Y.-F., Deng, J.-Y., Bi, L.-J., and Zhang, X.-E. (2008) Escherichia coli mismatch repair protein MutL interacts with the clamp loader subunits of DNA polymerase III. *Mutat. Res.* **637**, 101–110
11. Kadyrov, F.A., Dzantiev, L., Constatin, N., and Modrich, P.L. (2006) Endonucleolytic Function of MutLα in Human Mismatch Repair. *Cell* **126**, 297–308
12. Yang, W. (2007) Human MutLα: the jack of all trades in MMR is also an endonuclease. *DNA repair* **6**, 135–139
13. Nelson, K.E., Clayton, R.A., Gill, S.R., Gwinn, M.L., Dodson, R.J., Haft, D.H., Hickey, E.K., Peterson, J.D., Nelson, W.C., Ketchum, K.A., McDonald, L., Utterback, T.R., Malek, J.A., Linher, K.D., Garrett, M.M., Stewart, A.M., Cotton, M.D., Pratt, M.S., Phillips, C.A., Richardson, D., Heidelberg, J., Sutton, G.G., Fleischmann, R.D., Eisen, J.A., White, O., Salzberg, S.L., Smith, H.O., Venter, J.C., and Fraser, C.M. (1999) Evidence for lateral gene transfer between Archaea and bacteria from genome sequence of *Thermotoga maritima*. *Nature* **399**, 323–329
14. Ban, C. and Yang, W. (1998) Crystal structure and ATPase activity of MutL: implications for DNA repair and mutagenesis. *Cell* **95**, 541–552
15. Ban, C., Junop, M., and Yang, W. (1999) Transformation of MutL by ATP binding and hydrolysis: a switch in DNA mismatch repair. *Cell* **97**, 85–97
16. Konarev, P.V., Volkov, V.V., Sokolova, A.V., Koch, M.H.J., and Svergun, D.I. (2003) *PRIMUS*: a Windows PC-based system for small-angle scattering data analysis. *J. Appl. Crystallogr.* **36**, 1277–1282
17. Krukenberg, K.A., Forster, F., Rice, L.M., Sali, A., and Agard, D.A. (2008) Multiple Conformations of *E. coli* Hsp90 in Solution: Insights into the conformational Dynamics of Hsp90. *Structure* **16**, 755–765

18. Svergun, D.I. (1992) Determination of the regularization parameter in indirect-transform methods using percetual criteria. *J. Appl. Crystallogr.* **25**, 495–503
19. Svergun, D.I. (1999) Restoring low resolution structure of biological macromolecules from solution scattering using simulated annealing. *Biophys. J.* **76**, 2879–2886
20. Kozin, M.B. and Svergun, D.I. (2000) A software system for automated and interactive rigid body modeling of solution scattering data. *J. Appl. Crystallogr.* **33**, 775–777
21. Guarné, A., Romon-Maiques, S., Wolff, E.M., Ghirlando, R., Hu, X., Miller, J.H., and Yang, W. (2004) Structure of the MutL C-terminal domain: a model of intact MutL and its roles in mismatch repair. *EMBO J.* **23**, 4134–4145
22. Garnier, J., Gibrat, J.-F., and Robson, B. (1998) GOR secondary structure prediction method version IV. *Meth. Enzym., R.F. Doolittle Ed.* **266**, 540–553
23. Kozin, M. B. and Svergun, D. I. (2001) Automated matching high- and low-resolution structural models. *J. Appl. Crystallogr.* **34**, 33–41
24. Scott, D. J., Grossmann, J. G., Tame, J. R. H., Byron, O., Wilson, K. S., and Otto, B. R. (2002) Low Resolution Solution Structure of the Apo form of *Escherichia coli* Haemoglobin Protease Hbp. *J. Mol. Biol.* **315**, 1179–1187
25. Rasmussen, L. C. V., Oliveira, C. L. P., Jensen, J. M., Pedersen, J. S., Sperling-Petersen, H. U., and Mortensen, K. K. (2008) Solution structure of C-terminal Escherichia coli translation initiation factor IF2 by small-angle X-ray scattering. *Biochemistry* **47**, 5590–5598